Title

Cell cycle and lineage progression of neural progenitors in the ventricular-subventricular zones of adult mice.

Journal

Proceedings of the National Academy of Sciences of the United States of America, 110(11)

ISSN

0027-8424

Authors

Ponti, Giovanna
Obernier, Kirsten
Guinto, Cristina
et al.

Publication Date

2013-03-01

DOI

10.1073/pnas.1219563110

Peer reviewed

Cell cycle and lineage progression of neural progenitors in the ventricular-subventricular zones of adult mice

Giovanna Ponti[a,b], Kirsten Obernier[a], Cristina Guinto[a], Lingu Jose[a], Luca Bonfanti[b], and Arturo Alvarez-Buylla[a,1]

[a]Department of Neurological Surgery and The Eli and Edythe Broad Center of Regeneration Medicine and Stem Cell Research, University of California, San Francisco, CA, 94143; and [b]Department of Veterinary Sciences and Neuroscience Institute Cavalieri Ottolenghi, University of Turin, 10043 Turin, Italy

Edited by Pasko Rakic, Yale University, New Haven, CT, and approved January 23, 2013 (received for review November 9, 2012)

Proliferating neural stem cells and intermediate progenitors persist in the ventricular-subventricular zone (V-SVZ) of the adult mammalian brain. This extensive germinal layer in the walls of the lateral ventricles is the site of birth of different types of interneurons destined for the olfactory bulb. The cell cycle dynamics of stem cells (B1 cells), intermediate progenitors (C cells), and neuroblasts (A cells) in the V-SVZ and the number of times these cells divide remain unknown. Using whole mounts of the walls of the lateral ventricles of adult mice and three cell cycle analysis methods using thymidine analogs, we determined the proliferation dynamics of B1, C, and A cells in vivo. Achaete-scute complex homolog (Ascl)1$^+$ C cells were heterogeneous with a cell cycle length (T_C) of 18–25 h and a long S phase length (T_S) of 14–17 h. After C cells, Doublecortin$^+$ A cells were the second-most common dividing cell type in the V-SVZ and had a T_C of 18 h and T_S of 9 h. Human glial fibrillary acidic protein (hGFAP)::GFP$^+$ B1 cells had a surprisingly short Tc of 17–18 h and a T_S of 4 h. Progenitor population analysis suggests that following the initial division of B1 cells, C cells divide three times and A cells once, possibly twice. These data provide essential information on the dynamics of adult progenitor cell proliferation in the V-SVZ and how large numbers of new neurons continue to be produced in the adult mammalian brain.

adult neurogenesis | circadian rhythm | subependymal | thymidine analogs toxicity | transit amplifying progenitors

Neurogenesis continues along the walls of the lateral ventricle in the adult rodent brain. Neural stem cells correspond to a subpopulation of local astrocytes (B1 cells) (1–3), which retain an apical contact with the ventricle. Therefore, this adult germinal layer includes not only a subventricular component but also a ventricular zone [i.e., ventricular-subventricular zone (V-SVZ) (4)]. B1 cells give rise to intermediate progenitors or transit-amplifying cells (C cells), which divide to generate neuroblasts (A cells) that continue to proliferate (5–7) and migrate tangentially along the rostral migratory stream to the olfactory bulb, a process of continuous neuronal replacement that occurs throughout life (8–10).

Although the lineage in the V-SVZ has been determined, the cell cycle dynamics of each cell population remain unknown. An essential amplifying stage within the lineage is the proliferation of C and A cells. Small changes in the cell cycle length or number of times that these intermediate precursors divide could result in significant changes in the number of neurons produced. Previous studies estimated cell cycle dynamics for all dividing cells, assuming a homogeneous population. Moreover, the calculated length of the cell cycle (T_C) for all V-SVZ cells varies in different publications, from 13 to 14 h (11) or 18–21 h (12–14). Lengths of the S phase (T_S) as short as 4 h (11) or as long as 8.5–13 h (12–14) have also been reported. These variabilities might be explained not only by the pooling of all proliferating V-SVZ cells but also because these previous studies are based on the analysis of tissue sections. Neuroblasts continue to divide as they actively migrate tangentially (5, 15). Therefore, dividing cells move in and out of the counting bin in coronal or sagittal sections, likely introducing errors in the analysis (16).

Here, we estimated the cell cycle dynamics of V-SVZ progenitors in vivo using multiple methods and a whole-mount preparation that does not require sectioning (17). The spatial localization of neural stem cells determines the subtypes of olfactory bulb interneurons produced (18, 19); however, we found that the cell cycle dynamics were very similar across different subregions of the V-SVZ (see Fig. S2 *G–J*). Interestingly, our results indicate that actively dividing neural stem cells had a surprisingly short S phase. C cells had a much longer T_S, and their cell cycle dynamics were heterogeneous. Our data further indicate that during lineage progression, C cells divided approximately three times and A cells once or twice. This analysis reveals the in vivo dynamics of cell proliferation and neuronal production in this major adult germinal layer.

Results

Overall Estimates of Cell Types Dividing in the Adult V-SVZ. To label dividing cells during S phase, we used thymidine analogs 5-chloro-2′-deoxyuridine (CldU) (20, 21) and 5-ethynyl-2′-deoxyuridine (EdU) (22), which we found can be readily detected with similar sensitivity and without cross-reactivity (*SI Technical Notes*). However, we observed that EdU had long-term toxicity (Fig. S1 *B–I*), and, therefore, only used EdU for short-term labeling experiments.

Three markers were used for identification of the different proliferating progenitors in the V-SVZ: glial fibrillary acidic protein (GFAP) for B1 cells, Achaete-scute complex homolog (Ascl)1 for C cells (23), and doublecortin (DCX) for A cells (24). Because GFAP antibodies primarily stain the processes of B1 cells, we used hGFAP::GFP mice (25, 26), which express GFP under the control of the human GFAP promoter (Fig. 1*A*). In these mice, a small fraction ($1.90 \pm 0.15\%$; $n = 14$) of GFP labeled cells also stained for Ascl1 (Fig. 1*J*). Conversely, a small subpopulation ($3.07 \pm 0.57\%$; Fig. 1*K*) of Ascl1$^+$ cells were also positive for GFP. This population could correspond to a transitional stage in the lineage (27, 28) or to a population of long-term self-renewing neural

Significance

The time taken by neural stem cells and intermediate progenitor cells to transit through the cell cycle, and number of times they divide, is essential information to understand how new neurons are produced in the adult rodent brain.

Author contributions: G.P. and A.A.-B. designed research; G.P., K.O., C.G., and L.J. performed research; G.P. and A.A.-B. analyzed data; and G.P., K.O., L.B., and A.A.-B. wrote the paper.

The authors declare no conflict of interest.

This article is a PNAS Direct Submission.

Freely available online through the PNAS open access option.

[1]To whom correspondence should be addressed. E-mail: abuylla@stemcell.ucsf.edu.

This article contains supporting information online at www.pnas.org/lookup/suppl/doi:10.1073/pnas.1219563110/-/DCSupplemental.

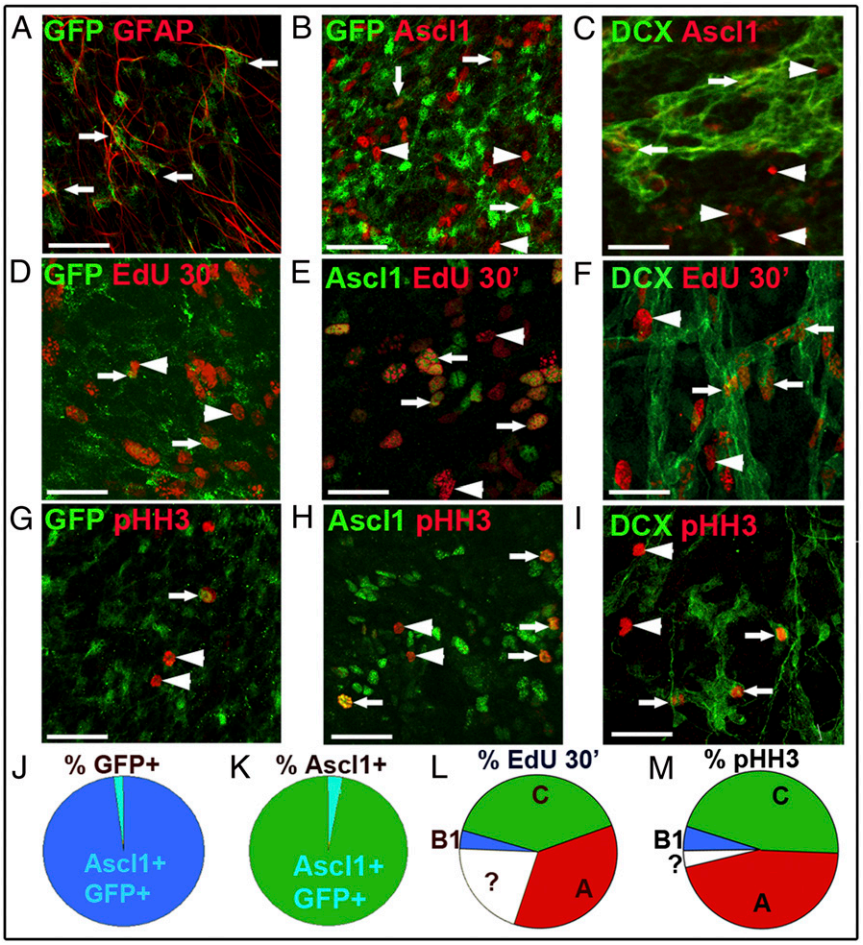

Fig. 1. Characterization of dividing cells in the V-SVZ. Confocal analysis of whole mounts of the lateral wall of the lateral ventricle with examples of cells stained for different markers. In hGFAP::GFP mice, the majority of GFP$^+$ cells were stained for GFAP (*A*). A small fraction of cells expressed both GFP and Ascl1 (*B*); for quantifications, *Results* and *J* and *K*). Also, a small fraction of Ascl1$^+$ cells expressed DCX (*C*). Thirty minutes (′) after EdU injection, a small fraction of EdU$^+$ cells expressed GFP (in hGFAP::GFP mice (*D*), whereas the majority expressed Ascl1 (*E*) or DCX (*F*); for quantification, see *Results* and *L*. Consistently, the fraction of GFP$^+$ cells (in hGFAP::GFP mice) labeled by mitotic marker pHH3 was small (*G*). Most of the pHH3$^+$ cells were either Ascl1$^+$ (*H*) or DCX$^+$ (*I*); for quantification, see *Results* and *M*. (Scale bars: 50 μm.) Arrows indicate double-labeled cells; arrowheads indicate single-labeled cells. (*L–M*) A fraction (labeled "?") of EdU$^+$ or pHH3$^+$ did not express GFP (B1 cells), Ascl1(C cells), or DCX (A cells) markers. (*D–F* and *L*) Thirty minutes after EdU injection. Means (n = 3) ± SEM.

stem cells that express Ascl1 (29), or both. The expression of Ascl1 was also retained in a subpopulation of DCX$^+$ cells: 15.87 ± 1.64% of the Ascl1$^+$ cells were DCX$^+$ (10.67 ± 3.12% of DCX$^+$ cells were Ascl1$^+$; n = 3).

We first determined the number of cells of the different types in the S phase using V-SVZ whole mounts. Following a single injection of EdU (30 min survival), GFP$^+$ cells accounted for 3.92 ± 0.91%, (n = 5), Ascl1$^+$ for 40.06 ± 1.78%, (n = 4), and DCX for 35.79 ± 2.09% (n = 3) of EdU$^+$ cells (Fig.1 *D–G*). We next quantified the percentage of mitotic cells [identified by phosphohistone H3 (pHH3) staining] among hGFAP::GFP$^+$, Ascl1$^+$, and DCX$^+$ cells. Consistent with the EdU labeling, the majority of pHH3$^+$ cells in the V-SVZ corresponded to Ascl1$^+$ (45.89 ± 0.08%; n = 60) and DCX$^+$ (45.57 ± 2.66%; n = 7) cells. hGFAP::GFP$^+$pHH3$^+$ were less common (4.80 ± 0.45%; n = 20; Fig. 1 *D* and *L*). Because quantifications of proliferating cells based on EdU incorporation or pHH3 staining may be affected by the length of T_S and mitosis (T_M) with respect to T_C, we also stained whole mounts with Ki67, a proliferation marker that is expressed throughout most of the cell cycle except G_0 (30). We found that for all Ki67$^+$ cells, 54.01 ± 3.22% were Ascl1$^+$, 53.52 ± 2.54% were DCX$^+$, and 3.30 ± 0.95% were GFP$^+$ (in hGFAP::GFP mice). Together, these results indicate that in the adult V-SVZ, proliferating Ascl1 and DCX$^+$ cells are both much more common than dividing hGFAP::GFP$^+$ cells.

We also counted the number of pHH3 or EdU (30 min survival) labeled Ascl1 and hGFAP::GFP$^+$ cells during different times of day and night (Fig. S2 *A–E* and *SI Technical Notes*). We found that the rate of proliferation for these two populations in the V-SVZ cells remained relatively constant with the circadian rhythm.

Actively Dividing hGFAP::GFP Cells Complete the Cell Cycle in Less than a Day. ***B1 cells: Cumulative labeling method.*** hGFAP::GFP mice received 1–16 injections of EdU (1 injection every 2 h) and were killed 30 min after the last injection. The total number of GFP$^+$ cells remained constant at all survival times studied, indicating that EdU injections did not affect the total number of GFP$^+$ cells within the V-SVZ (Fig. 2).

The labeling index (LI) (the number of double labeled cells divided by the total number of GFP$^+$ cells; n = 5) progressively increased up to 14 h, reaching a plateau with a LI of y = 0.08610. This corresponds to the growth fraction (GF), indicating that 8.6% of the GFP$^+$ population is actively proliferating (Fig. 2 *A–E*).

The data (Fig. 2*D*) can be described by two regression lines: "a," the linear increase in cell labeling between 30 min and 14 h (y = 0.00486 × +0.02186); and "b," the horizontal line between 14 and 24 h. The time (in the x axis) when the two regression lines intersect equals $T_C - T_S$ = 13.22 h. The intersect of line a with the y axis is defined as the initial labeling index (LI_0) and corresponds to GF × T_S/T_C (16, 31). For our data, LI_0 was 0.022. From these three equations, we calculated a T_C of 17.73 h and a T_S of 4.50 h for GFP$^+$ cells. Because the plateau (the intersect between lines a and b) is reached when all dividing GFP$^+$ cells have incorporated EdU, this method over-represents the population of cycling cells with the slowest T_C (32, 33). For this reason, 17.73 h is likely a reflection of the GFP$^+$ cells that take the longest time to complete the cell cycle.

B1 cells: Double thymidine analog method. We next used the double thymidine analog (DA) method (31, 32) to determine T_S for the GFP$^+$ cells. We labeled GFP$^+$ cells in S phase with an initial injection of CldU followed 2 h later by an injection of EdU and a

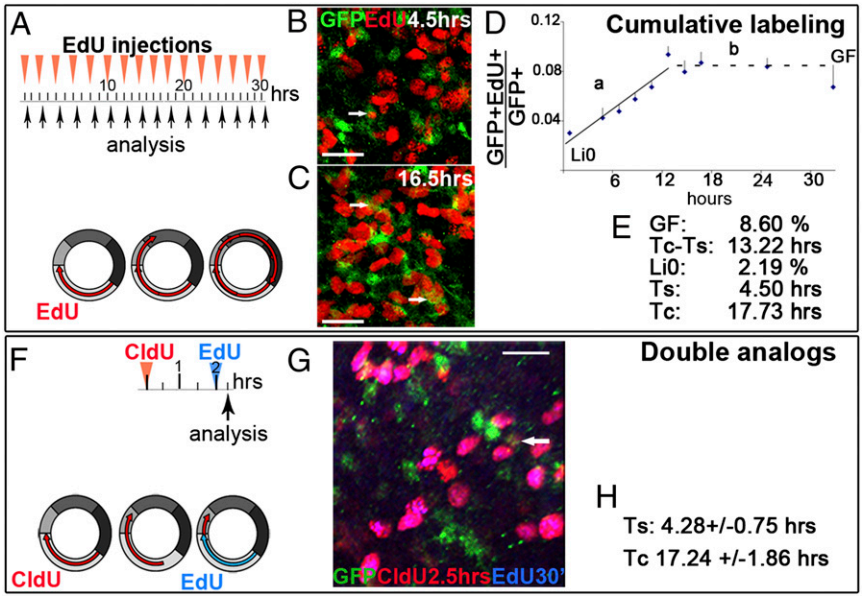

Fig. 2. Length of cell cycle phases for hGFAP::GFP$^+$ cells. (*A–E*) CL method. (*A*) Experimental outline; hGFAP::GFP mice received 1–16 injections of EdU every 2 h and were analyzed 30 min after the last injection (n = 5). (*B* and *C*) Confocal analysis of whole mounts of the lateral wall of the lateral ventricle. After three injections (4.5 h), only 4.2 ± 0.8% GFP$^+$ cells were EdU$^+$ (arrow) (*B*), whereas after nine injections (16.5 h), the percentage of GFP$^+$EdU$^+$/GFP$^+$ cells increased significantly to 8.7 ± 0.9% (n = 3; P = 0.0096; arrows) (*C*). (*D*) The ratio of double labeled cells within the GFP$^+$ population increased over time, reaching a plateau at 13.22 h when the entire cycling population (GF) entered the S phase (diagram). Least-square fit for line a: $y = 0.005 \times +0.022$; $R^2 = 0.897$; GF = 0.086. (*E*) Values for cells cycle parameters measured by CL. (*F–H*) DA method. (*F*) Experimental outline; mice received an injection of CldU and 2 h later EdU; analysis 30 min after EdU (n = 3). GFP$^+$CldU$^+$EdU$^-$ cells have exited the S phase, whereas EdU$^+$ cells are in S phase (diagram). (*G*) Confocal microscopy of triple-labeled cell (arrow). (*H*) Quantification of T_S and T_C by the DA method. (Scale bars: 25 μm.) Means (n = 3) ± SEM.

final survival of 30 min (Fig. 2 *F–H*; n = 5; see control experiments for EdU and CldU specificity in *SI Technical Notes*). Cells labeled by CldU, but not EdU (GFP$^+$CldU$^+$EdU$^-$) had left S phase. The ratio of GFP$^+$CldU$^+$EdU$^-$ cells over the total number of cells in the S phase (GFP$^+$EdU$^+$) equals 2 h/T_S. This ratio in five mice studied was: 0.50; 0.83; 0.33; 0.33; 0.67. Therefore, the average T_S = 4.28 ± 0.75 h. The ratio between the number of cells in S phase (GFP$^+$EdU$^+$) and the total GFP$^+$ proliferating population (GFP$^+$Ki67$^+$ cells) is proportional to the ratio T_S/T_C (31). We estimated this ratio for each animal (0.21; 0.29; 0.27; 0.25; 0.18) and calculated an average T_C = GFP$^+$Ki67$^+$ cells × T_S/GFP$^+$EdU$^+$ = 17.24 ± 1.86 h.

Because the DA method focuses on the initial cohort of cells exiting the S phase, it over-represents the fastest cycling cells. T_S and T_C calculated by both the DA and cumulative labeling (CL) methods were similar, suggesting that the population of actively dividing B1 cells is fairly homogeneous.

We next applied the percentage of labeled mitoses (PLM) method (33) for B1 cells (for a detailed description of the PLM method see below and Fig. 3*L*). hGFAP::GFP mice received a single injection of CldU and were analyzed at survivals ranging between 30 min and 8 h for the number of triple-labeled (GFP$^+$pHH3$^+$CldU$^+$) cells. Given the low number of GFP$^+$pHH3$^+$ B1 cells in our material, we only analyzed the period from the initial appearance of mitotic B1 cells to the time when all of these cells were triple-labeled. No triple labeled cells were observed at 30 min suggesting that $T_{G2} \geq$30 min. As CldU$^+$GFP$^+$ cells completed G_2, the number of mitotic GFP$^+$pHH3$^+$CldU$^+$ cells increased reaching 100% by 6 h (Fig. S1*W*). This indicates that G_2 phase length (T_{G2}) + T_M for hGFAP::GFP cells is ≤6 h. We did not use the PLM method to estimate T_C and T_S for B1 cells (*Discussion*).

Ascl1$^+$ Cells Are Heterogeneous in Their Cell Cycle Dynamics. Ascl1$^+$ nuclei were found in the V-SVZ under the ependymal layer. The majority of Ascl1$^+$ cells were actively proliferating; 52% of Ascl1$^+$ cells were labeled 30 min after a single EdU injection, and a large fraction of Ascl1$^+$ cells (89.15 ± 1.72%) was labeled by Ki67. The majority of Ascl1$^+$ cells correspond to actively dividing intermediate progenitors C cells (23).

C cells: CL method. Wild type mice received 1–10 injections of EdU (separated by 2 h intervals; n = 5 for each time point) and were killed 30 min after the last injection (*Materials and Methods* and Fig. 3 *A–D*). As with the B1 cells, the total number of Ascl1$^+$ cells remained constant for all time points studied, indicating that EdU was not toxic to Ascl1$^+$ cells for the duration of the CL experiment. The LI of Ascl1$^+$ cells progressively increased up to 10 h before reaching a plateau. We used two regression lines (a and b) and calculated the GF, LI_0, and $T_C - T_S$ (Fig. 3 *A–D*) using the same method as indicated above for hGFAP::GFP cells. The GF (87.11 ± 0.46%) calculated by the CL was similar to the ratio of Ascl1$^+$Ki67$^+$/Ascl1$^+$ cells (89.15 ± 1.72%; P = 0.47; n = 5). Using the equations described above for the hGFAP::GFP$^+$ cells, we calculated T_C = 25.44 h and T_S =14.80 h for the Ascl1$^+$ population.

C cells: DA method. Mice received one injection of CldU followed by an injection of EdU 3 h later. Thirty minutes after EdU, mice were killed, and the number of Ascl1$^+$CldU$^+$EdU$^-$ cells (cells that have exited the S phase between the two injections) was quantified in whole mounts (Fig. 3 *E* and *F*). We also counted the number of Ascl1$^+$EdU$^+$ labeled cells (in S phase) and from the ratio of Ascl1$^+$CldU$^+$EdU$^-$/Ascl1$^+$EdU$^+$ cells (n = 5; 0.20; 0.19; 0.21; 0.27; 0.22), we calculated the average T_S = 12.20 ± 1.56 h. We next used the percent of Ki67$^+$Ascl1$^+$ cells (89.15 ± 1.72%) as an estimate of the population of Ascl1$^+$ cells that is actively dividing to determine the average T_C = 18.21 ± 4.15 h (Fig. 3 *E* and *F*). Consistent with the observations made above using the CL method, these data show that Ascl1$^+$ cells have a long T_S. Given how long C cells remain in the S phase, this method may overestimate T_S. We, therefore, used an additional method to determine cell cycle dynamics for the Ascl1 population.

C cells: PLM. To estimate T_S and T_C with a different approach and determine T_{G2}, T_M, and G_1 phase length (T_{G1}), we used the PLM method (33). Mice received a single CldU injection and were killed at different time points (n = 5 for each time point). Whole mounts of the V-SVZ were stained for Ascl1, CldU, and the mitotic marker pHH3. The number of pHH3$^+$Ascl1$^+$ cells was constant for all time points studied, indicating that neither experimental manipulations nor the incorporation of CldU interfered with the cell cycle dynamics of Ascl1$^+$ cells (Fig. S2 *E*). For each time point, we calculated the ratio of pHH3$^+$Ascl1$^+$CldU$^+$/Ascl1$^+$pHH3$^+$ cells (Fig. 3 *G–K*) (33). Thirty minutes after the CldU injection, CldU$^+$Ascl1$^+$ cells were all pHH3$^-$, indicating that this cohort of CldU-labeled cells had not entered mitosis (Fig. 3*L*). As this cohort transitioned through G_2 and entered mitosis, triple-labeled cells appeared, reaching 100% at T = T_{G2} + T_M. From regression line a (Fig. 3*L*), we determined T_{G2} = 0.92 h (y = 0) and T_M = 3.27 h

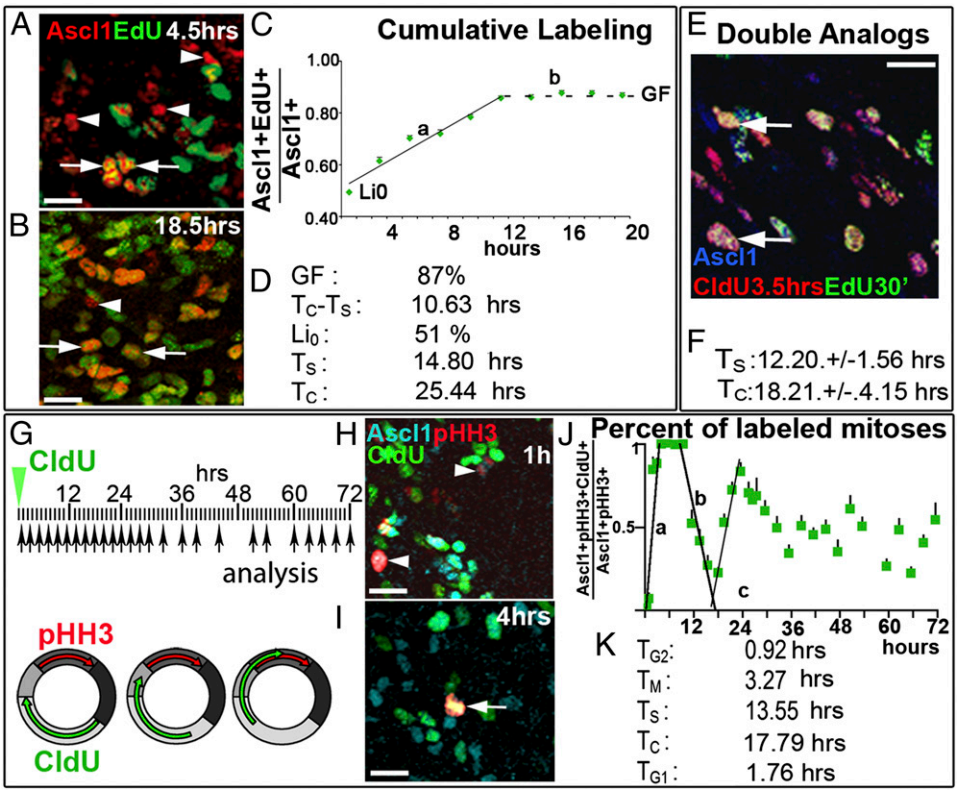

Fig. 3. Length of cell cycle phases for Ascl1$^+$ cells. For experimental outlines, see Fig. 2. (*A–D*) CL method. (*A* and *B*) Confocal analysis of whole mounts of the lateral wall of the lateral ventricle. After three injections (4.5 h), 70.99 ± 1.67% of Ascl1$^+$ cells were labeled with EdU (arrows) (*A*); after 18.5 h 86.70 ± 1.16%, Ascl1$^+$ cells were double-labeled (*B*). (*C*) Ratio of Ascl1$^+$EdU$^+$/Ascl1$^+$ cells increased with additional injections of EdU reaching a plateau at 10.63 h when the entire cycling population (GF) has entered the S phase. (*D*) Cell cycle values as determined cell cycle parameters quantified by the CL; Least square fit; line a: y = 0.034 × +0.506; R^2 = 0.966; GF = 0.87. (*E* and *F*) DA method. (*E*) Confocal microscopy of triple-labeled cells (arrows). (*F*) Quantification of T_S and T_C by the DA method. (*G–M*) PLM method. (*G*) Experimental outline; C57/BL6 mice received an injection of CldU and were analyzed for pHH3$^+$ mitoses at different times (n = 5) . (*H* and *I*) Confocal analysis of whole mounts of the lateral wall of the lateral ventricle after 1 h (*H*) or 4 h (*I*) after CldU (Ascl1$^+$pHH3$^+$ cells; arrowhead, Ascl1$^+$pHH3$^+$CldU$^+$ cell; arrow). (*J*) The ratio of triple labeled cells (Ascl1$^+$pHH3$^+$CldU$^+$) over the pHH3$^+$Ascl1$^+$ increased, reaching a plateau when the last CldU labeled cell exited mitosis. The fraction of labeled mitosis decreased during G_1 but increased again as CldU$^+$ cells reentered mitosis. Least-square fit; line a, y = 0.306 × −0.281 (R^2 = 0.836); line b, y = −0.115 × +2.040 (R^2 = 0.880); line c: y = 0.140 × −2.348 (R^2 = 0.958). (*K*) Cell cycle phases quantified by PLM. (Scale bars: 25 μm.)

(y = 1). A second regression line b describes the progressive decrease in triple-labeled pHH3$^+$Ascl1$^+$CldU$^+$ cells as the cohort of cells that incorporated CldU has completed mitosis and entered G_1. The minimum is reached when the last CldU-labeled cell exited mitosis. The interval between the time in which the first and the last Ascl1$^+$CldU$^+$ cell exited mitosis corresponds to T_S = 13.55 h. When CldU labeled cells reentered mitosis for a second time, triple-labeled cells appeared again ("c"). The total T_C can be measured by the time interval between two corresponding points (the midpoint) on the two ascending lines (33). Therefore, from a and c, we determined T_C = 16.79 (*Materials and Methods*). T_{G1} can be approximated to be 1.76 h, by the subtraction of T_S + T_{G2} + T_M from T_C (34). This is about 10% of T_C. Considering that the GF for C cells was 87%, about 8.7% of all C cells in the V-SVZ should be in G_1 phase at any one time.

The time estimated for each cell cycle phase by the PLM method corresponds to the fastest dividing Ascl1$^+$ cells (rising time, the slope in line a). The falling time course b is a reflection of the slower trailing population (33). The difference between the rising time and the falling time was 5.42 h, corresponding to 32% of T_C for the rapidly dividing population. From this, we estimated that the T_C varied between 16.78 and 22.21 h and T_S between 13.55 and 17.92 h.

About one-fourth of the population of Ascl1$^+$ cells appears to be asynchronous since the second peak of triple-labeled CldU$^+$Ascl1$^+$pHH3$^+$ cells, indicating cells undergoing a second cell cycle, reached only 75%. Consistent with the heterogeneity of T_C for the Ascl1$^+$ population, the number of triple-labeled cells at time points longer than 30 h became highly variable. However, a third peak is clearly discernible at about 50 h, as expected for a third division of Ascl1$^+$ cells with a T_C of <20 h (Fig. 3*L*).

The three methods used indicate that Ascl1$^+$ cells have a surprisingly long T_S (~14–18 h). Interestingly, Ascl1$^+$ cells are heterogeneous with respect to the length of T_C. Different types of neurons are derived from unique subregions of the postnatal and adult V-SVZ (18, 35). Variability in the proliferation dynamics between regions could account for the observed heterogeneity. The posterior V-SVZ had a slightly higher GF (by CL) and a slightly longer T_C compared with the anterior V-SVZ (Fig. S2 *G–J*). However, T_C or the lengths of the different cell cycle phases of Ascl1$^+$ cells between these subregions was remarkably similar, suggesting that the heterogeneity observed among Ascl1$^+$ cells occurs throughout the V-SVZ and is likely attributable to other factors (*Discussion*).

Neuroblasts Continue to Divide with Cell Cycle Dynamics Similar to Those of Fast Cycling C Cells. We next investigated the cell cycle parameters of the DCX$^+$ cells (neuroblasts, A cells). It has been shown previously that A cells continue to divide while migrating

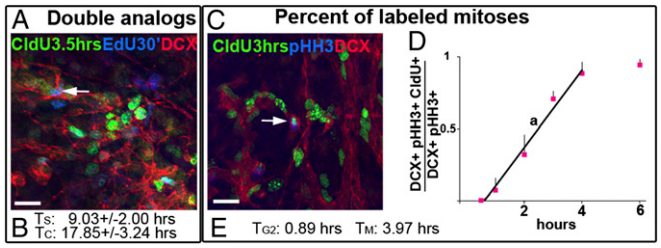

Fig. 4. Length of cell cycle phases for DCX$^+$ cells. (*A* and *B*) DA method; for experimental outline, see Fig. 2*F*. Confocal analysis at 3.5 h (triple-labeled cell; arrow). (*B*) T_S and T_C determined by DA. (*C*–*E*) Short PLM method (for experimental outline see Fig. 3*G*). (*C*) Confocal analysis 3 h after CldU (triple-labeled cell; arrow). (*D*) Ratio of triple-labeled cells (DCX$^+$pHH3$^+$CldU$^+$) to mitotic DCX$^+$ cells. (*E*) T_{G2} and T_M quantified by PLM Least square fit; line a, $y = 0.268 \times -0.168$; $R^2 = 0.985$. The CL method and the long version of PLM cannot be reliably used for DCX$^+$ cells because of their active tangential migration (*Results*). (Scale bars: 25 μm.)

(15, 36); we observed that 54.63% (±1.26%; $n = 3$) of the DCX$^+$ cells were positive for Ki67 (Fig. 1).

Because A cells migrate rapidly away from the walls of the ventricle into the dorsolateral corner of the V-SVZ and into the rostral migratory stream, the proportion of labeled cells within our counting bin changes over time. For this reason, methods that use long survivals (CL and long-term PLM) cannot be reliably used to calculate cell cycle dynamics of A cells (16). We, therefore, used strategies that use short survivals: the DA method and a short version of the PLM technique.

A cells: DA method. C57/BL6 mice received one injection of CldU followed by an injection of EdU 3 h later. Mice were analyzed 30 min after EdU injection ($n = 3$). At this time, 30.46 ± 2.33% of all DCX$^+$ cells were labeled by EdU ($n = 3$; Fig. 1), whereas 10.42 ± 2.79% were labeled by CldU but not by EdU. For each animal, we calculated the ratio of DCX$^+$CldU$^+$EdU$^-$ to DCX$^+$EdU$^+$ ($n = 3$; 0.26; 0.29; 0.58) and estimated T_S (see above; Fig. 4*A*; average $T_S = 9.03 \pm 2.00$ h).

The ratio of DCX$^+$EdU$^+$ cells to DCX$^+$Ki67 cells equals the ratio of T_S to T_C. We estimated this ratio for each animal (0.48; 0.56; 0.38) and calculated the average $T_C = 17.85 \pm 3.24$ h.

A cells: PLM short method. We analyzed the initial appearance of mitosis among cells that had incorporated CldU following a single injection (50 mg/kg). The number of mitotic (pHH3$^+$) CldU$^+$DCX$^+$ triple-labeled cells was determined after 30 min and 1, 2, 3, 4, and 6 h ($n = 3$ each time point). Thirty minutes after injection, we did not observe any DCX$^+$ cells that were labeled by CldU (0 out of 47 DCX$^+$pHH3$^+$ cells counted; $n = 4$). In contrast, the majority of DCX$^+$pHH3$^+$ cells were CldU$^+$ at 5 and 6 h postinjection (88.10 ± 7.90% and 88.54 ± 6.93%,

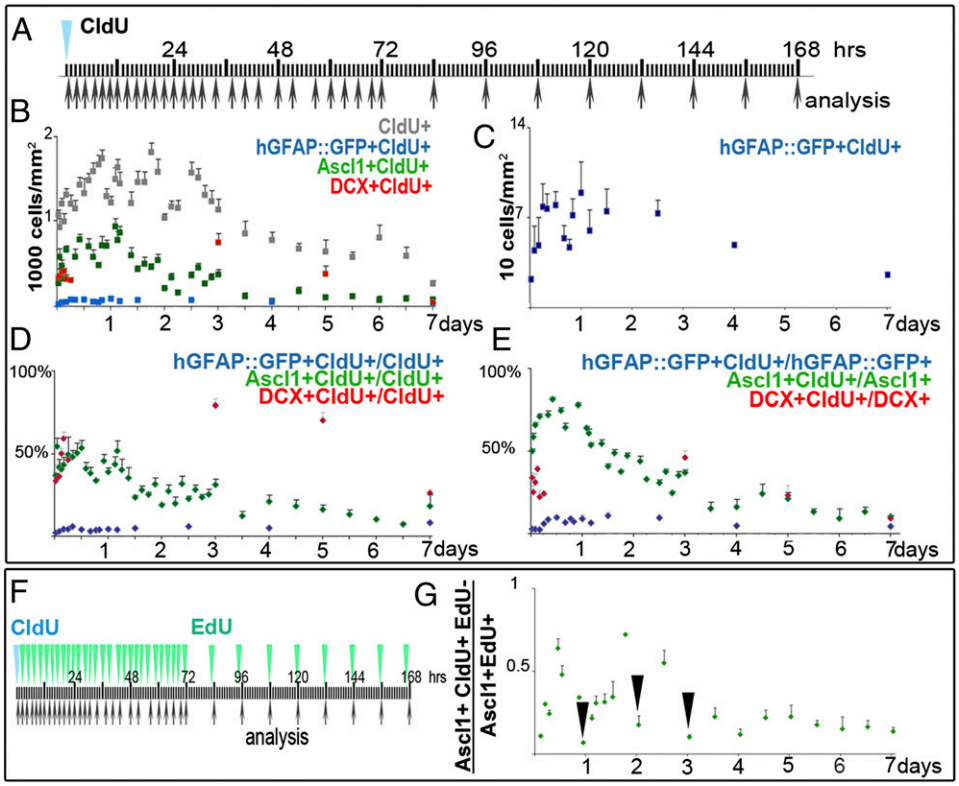

Fig. 5. Ascl1$^+$ cells divide 3–4 times before differentiating into neuroblasts. (*A*) Experimental outline: C57/BL6 or hGFAP::GFP mice received one injection of CldU at $t = 0$ and were analyzed at different time points ($n = 3$). (*B*) Numbers of CldU$^+$, Ascl1$^+$CldU$^+$, hGFAP::GFP$^+$CldU$^+$, and DCX$^+$CldU$^+$ cells/mm^2 over time; analyzed as whole mounts. All CldU$^+$ and Ascl1$^+$CldU$^+$ cells increased during the first day as the labeled cells underwent mitosis, and then numbers remained high for ~3 d for all CldU$^+$ cells and for ~1.5 d for the Ascl1$^+$CldU$^+$ population. We analyzed fewer time points for the DCX$^+$CldU$^+$ cells, but for this population, the highest value was observed 3 d after CldU. At all time points, only a small fraction of all CldU$^+$ cells corresponded to hGFAP::GFP$^+$ cells; these cells increased in numbers during the first day, remained high for ~2.5 d, and decreased gradually at day 4 and 7 (*B*) (expanded scale in *C*). (*D*) Percentage of each cell type within the CldU-labeled population. Whereas labeled Ascl1$^+$ decreased with survival, DCX$^+$CldU$^+$ cells sharply increased. (*E*) Percentage of CldU$^+$ cells in each population. The percentage of labeled Ascl1$^+$ cells decreased progressively between 1 and 3 d, whereas labeled cells within the DCX$^+$ population increased during this period. (*F* and *G*). Evaluation of the number of times Ascl1$^+$ cells divide. (*F*) Experimental outline: C57/BL6 mice received one injection of CldU at $t = 0$ and one of EdU at different time points 30 min before the mice were killed. CldU$^+$EdU$^-$ cells were in S phase at $t = 0$, whereas EdU$^+$ cells were in S phase at time of analysis. (*G*) Ratio of Ascl1$^+$CldU$^+$EdU$^-$ cells to Ascl1$^+$EdU$^+$ cells varies cyclically according to the cell cycle of Ascl$^+$ cells and revealed three troughs (arrows, corresponding to one cell cycle) approximately 1 d apart.

respectively). From the slope of the regression line before reaching the plateau (first four values), we determined T_{G2} = 0.89 h and T_M = 3.97 h (Fig.4*B*). Thus, neuroblasts had a T_C, T_{G2}, and T_M similar to that of C cells but had a shorter S phase and a longer G_1 phase.

Intermediate Progenitors of the V-SVZ Divide on Average Three to Four Times. Amplification in the V-SVZ lineage is critically dependent on the number of times intermediate progenitors divide. Our PLM analysis suggests that some C cells divide at least two times and possibly three, but given the heterogeneity in T_C, it is difficult to determine whether additional divisions occur (Fig. 3). To better understand changes in the overall population of newly generated V-SVZ cells and infer a possible lineage progression, we injected CldU and counted the number of labeled hGFAP::GFP$^+$, Ascl1$^+$, and DCX$^+$ cells at different survivals (Fig. 5 *B* and *C*; n = 3–8 each time point). The number of CldU$^+$ cells (gray squares, 935 ± 80 cells/mm^2) increased in the first 18 h (Fig. 5*B*) as cells undergo mitosis; then they decreased and raised again at least three times. This suggests that the balance between addition of cells (by mitosis) and decrease (by migration, label dilution, and/or cell death) for the overall population is relatively stable during the first 2.5 d. Between 2.5 and 3 d, the population of CldU-labeled cells declined to a plateau of about 724 ± 56 cells/mm^2 that was maintained for the next 3.5 d. As expected, at all times studied, B1 cells only accounted for a small fraction (<5%; GFP$^+$; blue squares in Fig. 5 *B* and *D*) of dividing cells. Three hours after injection, 49.57 ± 2.73% of the CldU$^+$ cells were DCX$^+$ and 40.42 ± 3.05% were Ascl1$^+$. Over time, proliferating Ascl1$^+$ cells decreased and remained relatively low between day 3.5 until day 7 (13.29 ± 1.63% of the total CldU$^+$ population). This decrease was paralleled by an increase in DCX$^+$CldU$^+$ cells (79 ± 4% at 3 d; Fig. 5 *B* and *D*), suggesting that the decline in the overall population of CldU$^+$ cells between 2.5 and 3.5 d (Fig. 5*B*, gray squares) occurs because many of the labeled C cells give rise to A cells that rapidly move away from the V-SVZ (Fig. 5 *B* and *D*, green and red squares). Given the T_C calculated above for B1 and C cells, 2.5–3.5 d is sufficient for three to four divisions of these progenitors. CldU-labeled cells further decreased between 6.5 and 7 d as A cells continue to emigrate and their replenishment from labeled C cells and by their own divisions comes to an end. The rapid migration of A cells makes it difficult to determine how many times they divide. The overall numbers of A cells between 3.5 and 6.5 d remained relatively constant, suggesting that addition by conversion from C cells, their own mitoses and their depletion by CldU dilution, emigration, and cell death results in no appreciable accumulation in the V-SVZ. The proportion of A:C = 1.5:1 cells can be explained by a lineage tree where C cells divide three times and A cells divide once (Fig. 6). This is assuming little, or no, cell death or that cell death affects both populations equally.

To independently estimate the number of times intermediate progenitor (C cells) divide, we calculated the ratio of Ascl1$^+$ cells that were in S phase vs. Ascl1$^+$ cells in other phases of the cell cycle (G_2 + M + G_1) at different time points. Mice received one injection of CldU, followed by one injection of EdU at different intervals. Mice were killed 30 min after the EdU injection. CldU$^+$ cells correspond to cells that underwent S phase at t = 0, whereas cells labeled by EdU were in the S phase at the time animals were killed (n = 3 for each time point). Most Ascl1$^+$CldU$^+$ cells were also labeled by EdU when the interval between the two injections was 2 h (Fig. 5*G*). The number of Ascl1$^+$CldU$^+$EdU$^-$ cells increased as the cohort of CldU$^+$ cells exited the S phase. Between 10 and 22 h, the number of Ascl1$^+$CldU$^+$EdU$^-$ cells decreased as proliferating progenitors reentered the S phase and incorporated EdU. This time (22 h) is similar to the average T_C of Ascl1$^+$ cells determined above. Within the first 3 d, three troughs corresponding to sequential S phases could be detected (black arrows in Fig. 5*G*) and possibly a fourth one at day 4 (gray arrow in Fig. 5*G*). These data again indicate that C cells divide, with a cell cycle just short of 1 d, three to four times. However, one division is likely attributable to labeling of B1 cells that upon division gave rise to CldU$^+$Ascl1$^+$ C cells.

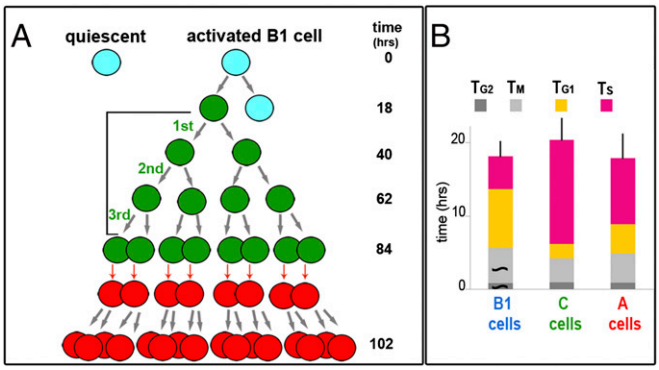

Fig. 6. Inferred lineage and cell cycle parameters for V-SVZ progenitor cells. Data suggest that after the initial division of GFAP$^+$ B1 cells, Ascl1$^+$ C cells divide three times and A cells once (possibly twice). Assuming no cell death, the asymmetric division of one B1 cell results in the generation of 16 (32) A cells; see *Discussion* for other assumptions and limitations of the analysis. (*A*, *Right*) Illustration of the V-SVZ lineage indicating amplification steps from a B1 cell (blue) through C cells (green) to A cells (red). Gray arrows, divisions; red arrows, differentiation. (*A*, *Left*) The calculated T_C, T_S, T_{G1}, and percentage of proliferating cells (GF of B1 and C cells from CLM; percentage of Ki67-labeled for A cells). (*B*) Graphical representation of the cell cycle phases in B1, C, and A cells. For B1 cells, the length of T_{G2} and T_M is approximate (~), given the low numbers of mitotic (pHH3$^+$) B1 cells present (Fig. S1*X*).

Discussion

Our results indicate that the T_C for the three main progenitor cells in the adult V-SVZ of adult mice was slightly shorter than 1 d (B1 cells: 17 h; C cells: ~18–25 h; A cells: 18h; Fig. 6), but the T_S for the actively dividing B1 cells was surprisingly short (4.5 h) compared with that of C cells (12–17 h) and A cells (9 h; Fig. 6). In this study, we only analyzed actively dividing GFAP$^+$ cells. We cannot exclude that there is a population of quiescent B1 cells with a longer T_C possibly associated with periods of quiescence (37). Interestingly, the short S phase and long G_1 phase of the actively dividing B1 cells is similar to that of radial glia (38), the neural stem cells in development, and the precursors of B1 cells (39). Our results suggest that following the initial division of GFAP$^+$ B1 cells, Ascl1$^+$ C cells divide three times before turning into DCX$^+$ A cells. Because A cells actively migrate as they divide, it is difficult to determine how many times they undergo cell division; our results suggest they may divide once or twice before leaving the V-SVZ.

Tools for Studying the Cell Cycle Dynamics and Their Limitations. Thymidine analogs have been instrumental to identify and follow the division of neural progenitors in the adult brain, but these analogs may label cells undergoing DNA repair or cell death (40, 41). Most, if not all, of the labeling we observed following EdU or CldU injections was associated with proliferation because: (*i*) at short survivals (30 min), EdU and CldU labeled similar ratios of the different cell types (hGFAP::GFP, Ascl1, and DCX) as mitotic marker pHH3 and proliferation marker Ki67; (*ii*) the population of dividing Ascl1$^+$ cells was similar using cumulative EdU labeling or Ki67. Toxicity for CldU or EdU was not observed at short survival times, consistent with previous reports (42). However, at longer survival times the numbers for CldU-labeled cells were much higher compared

with cells that incorporated EdU (Fig. S1 *B–I*). This suggests that EdU is toxic at longer survivals. Consistently, pyknotic nuclei were common among V-SVZ cells 1 d after EdU treatment but not in mice injected with CldU (Fig. S1 *B–I*). Toxic effects of EdU, but not CldU, were also observed in primary cultures from V-SVZ 24 h after treatment (Fig. S1 *B–I*). We, therefore, used EdU only in experiments shorter than 18 h and CldU in experiments that extended beyond the first cell cycle.

The estimation of cell cycle dynamics requires that dividing cells remain in the counting bin for the duration of the experiment (16); this condition is not met in sectioned brain tissue because A cells actively migrate tangentially. Earlier studies applying the CL method for the total dividing V-SVZ population in neonate (43) and adult mice report a shorter T_C of 12–14 h (11) compared with the present results and others' data (12, 14, 44). Those differences are likely attributable to the use of tissue sections in different planes, the migration of neuroblasts, and the heterogeneous nature of progenitors. We have attempted to overcome some of these limitations by the use of V-SVZ whole mounts. The *en face* view allows inclusion of a larger bin in a tangential plane. However, we can only reduce, but cannot eliminated, the effects of migration of neuroblasts because a subpopulation of these cells is constantly moving away from V-SVZ into the rostral migratory stream. For these reasons, we used only short survival methods (DA and first ascending slope in PLM) for the cell cycle analysis of A cells.

Identification of Dividing Progenitors in the Adult V-SVZ. Precise estimates of cell cycle dynamics in the adult V-SVZ require identification of the different types of dividing progenitors. We have used hGFAP::GFP mice to identify B1 cells and immunostaining for Ascl1 and DCX to label C and A cells, respectively (23, 26, 45). Most of the proliferating hGFAP::GFP$^+$ astrocytes within the V-SVZ are neural stem cells (1, 46) and express other astrocytic markers, such as Glutamate Aspartate Transporter (GLAST) (47) and Aldehyde dehydrogenase family 1 member L1 (Aldh1-L1)L1 (48). hGFAP::GFP mice reporter protein was more reliable for quantification of B1 cells than GLAST::DsRed (49) and AldH1-L1::GFP (50) (Fig. S1 *J–V*). However, among the cells identified with any of these markers, including the hGFAP-GFP mice, there is also a small population of V-SVZ astrocytes that are non-neurogenic, and we cannot exclude possible effects of this population from our analysis.

Because, in our study, the majority of cells studied correspond to singly labeled populations, we believe that our data reliably reflect the cell cycle dynamics of major progenitor stages in the V-SVZ. However, progenitor cells are dynamic and constantly drifting to a new stage of differentiation and, therefore, stable progenitor stages may not exist in vivo, possibly explaining some of the heterogeneity we observe (see below). Consistently, we observed a few cells that express markers for two cell types, hGFAP::GFP and Ascl1 (B1 and C cell markers) or Ascl1 and DCX (C and A cells). The population of cells double-labeled by hGFAP::GFP and Ascl1 was small (<3%). In "knock-in" Ascl1::inducible Cre (Cre recombinase fused to a mutant estrogen ligand binding domain, CreERT2)$^{/+}$ mice, the reporter is expressed mainly in intermediate progenitors and in a small subset of neural stem cells (29). In another study, 36% of GFAP$^+$EGFR$^+$ cells are found faintly Ascl1$^+$ (28), suggesting that the expression of EGFR may be associated with this transitional stage. Interestingly, about 11% of Ascl1$^+$ cells were also DCX$^+$. This suggests that newly generated cells that have begun neuronal differentiation may retain some features associated with the intermediate progenitor stage including proliferation for some period of time.

Ascl1, which activates expression of the proneurogenic program, also has pivotal roles in promoting the G_1-to-S and G_2-to-M transitions (23, 51). During development Ascl1 and Hes1 oscillate in opposite directions during the cell cycle with high Hes1 expression in G_1 (52). If Ascl1 also fluctuates in the adult V-SVZ, the fraction of C cells labeled by Ascl1 may vary along the cell cycle and we may have underestimated the total population of C cells. This may also explain the short G_1 in our PLM estimates (Fig. 6). The T_C of C cells may, thus, be somewhat longer than calculated.

Origin of C Cell Cycle Heterogeneity. Our data indicate that C cells are heterogeneous with a T_C that varied between 18 and 25 h. In the PLM analysis, the rising and falling dynamics during the first cycle (Fig. 5*L*) suggested a difference of about 5 h in T_C between the fastest and slowest dividing Ascl1$^+$ cells (33). This heterogeneity did not result from differences in the cell cycle dynamics in different subregions of the V-SVZ (Fig. S2 *G–J*). We found no significant changes in the number of cells incorporating EdU, nor in the number of mitotic pHH3$^+$ V-SVZ cells at different times of the day both for the hGFAP::GFP$^+$ and Ascl1$^+$ cells (Fig. S2 *A–E*). Instead, C cell's cell cycle heterogeneity could be attributable to differences in T_C between first generation C cells (those derived from B1) and subsequent generations. Interestingly, in vitro time-lapse recording reported a deceleration in the cell cycle as intermediate progenitors progress through the lineage (53).

Cell Cycle Dynamics and Lineage Progression. Our data suggest that following the division of B1 cells, there are three amplifying divisions associated with the proliferation of C cells, and one or two divisions associated with the division of A cells (Fig. 6). From our estimated cell cycle transit time, the generation of the initial C cells can occur in less than a day with the following amplification of C cells completed in 3.5–4 d. Consistent with previous reports (5–7), an important fraction of the proliferating cells in the V-SVZ corresponded to A cells. The additional division(s) of these neuroblasts further amplifies the number of new neurons as illustrated in Fig. 6. If A cells divide once or twice, it should take an additional 17–40 h to complete the lineage. This is a total of 4–6 d from the initial division of a B1 cell to the generation of postmitotic young neurons. This is consistent with the observations that during regeneration following antimitotic treatment, A cells are first observed at 4.5 d (54), and following a single CldU injection, the majority of proliferating cells leaves the V-SVZ after 6–7 d (Fig. 5).

The GF for hGFAP::GFP cells was 8.6%; these cells likely correspond to the population of activated B1 cells (28). We counted a total of 6,200 ± 200 hGFAP::GFP cells in the V-SVZ of 2-mo-old mice. Therefore, the number of dividing hGFAP::GFP cells in the V-SVZ at any one time is 533 ± 17 cells. With a T_C for B1 cells of ~17 h, we can extrapolate that in a day, about 711 ± 23 B1 cells divide in the V-SVZ. With this initial number of primary progenitors dividing every day, four amplifying divisions of intermediate progenitors should suffice to generate ~10,000 A cells, which is an estimated of the number of migrating young neurons that moves along the rostral migratory stream every day (5, 15), (Fig. 6*A*). This assumes no cell death or derivation of daughter cells into alternative lineages. Because there is some level of cell death (6, 11, 55) in the V-SVZ, and some of the progeny of intermediate proliferating progenitors is diverted into the production of oligodendrocytes (56, 57), we conclude that, on average, the neurogenic V-SVZ lineage from B1 to A cells likely includes four to five amplifying divisions (including those of C and A cells).

Consistent with our observations, a recent in vitro study suggests that slowly dividing primary astroglial progenitors divide asymmetrically to generate actively dividing cells that continue to express astroglial markers (53). The latter likely corresponds to the activated hGFAP::GFP cells that we studied here. Costa et al. (53) also found ~five stages of amplification, which should result in similar numbers of generated A cells from activated B1

cells, as calculated above. It is interesting that the behavior of isolated progenitors in vitro, without exposure to growth factors, is similar to that inferred here in vivo, further supporting the view that lineage progression may be largely cell-autonomously determined (53).

As discussed above, the average T_C for Ascl1$^+$ cells was slightly longer than the average T_C for B1 and A cells. T_M and T_{G2} were, however, comparable for all three types of progenitors. Interestingly, C cells had a T_S 3.5–4.3 fold as long as that of B1 cells and 1.4–2.1 fold longer than that of A cells (Fig. 6*B*). Pluripotent stem cells and immortalized cell lines also have proportionally longer T_S (58). Checkpoints in G_1 and S phases prevent the replication of damaged DNA (59) and slow down S-phase progression (60). It is possible that C cells undergo extensive DNA damage control, extending the T_S. Other factors, including slower rate of nucleotides synthesis (61), slower fork elongation during replication (62), or increased heterochromatin (63), could all contribute to a longer T_S (64).

Intermediate progenitors in the developing cortical SVZ also have a longer S phase compared with cortical VZ neural stem cells. Intermediate progenitors' long T_S could be associated with changes in the patterns of gene expression because these cells progress along the neurogenic lineage (see above). A change in gene expression may require dramatic epigenetic changes (64), and this may slow down cell cycle progression.

With the caveat discussed above of possible oscillation in Ascl1 expression, PLM experiments also suggest that C cells have a surprisingly short T_{G1}, shorter than those of A and B1 cells. During cortical development, T_{G1} is longer in primary apical progenitors compared with committed neuronal intermediate progenitors in the SVZ (65–67). It has been proposed that the time available during G_1 for the accumulation of cell fate factors determines whether the cell differentiates or reenters the cell cycle (65); a short T_{G1} may favor proliferation (68), whereas lengthening of G_1 may trigger differentiation (69). This is consistent with our observation that C cells have a very short T_{G1}, likely related to their repeated divisions before they begin neural differentiation into A cells.

Concluding Remarks

This study provides the dynamics of lineage progression from neural stem cells to their progeny in the adult brain. The study reveals a number of unexpected observations; a subpopulation of B1 cells was actively dividing, with a relatively short cell cycle compared with that of intermediate progenitors, C cells, which have long S and short G_1 phases. The work also highlights the importance of neuroblast division for the overall high number of new neurons produced in the adult V-SVZ. This also explains why A cells account for almost half of all actively dividing cells (Fig. 6). It is reassuring that our cell cycle estimates predict quite accurately the overall number of different types of dividing progenitors observed at any one time, the overall progression from one stage to the next, the total number of young neurons produced, and the timing of clearance of dividing cells from the V-SVZ as neuroblasts move into the rostral migratory stream and olfactory bulb. The cell cycle progression described here for the different progenitor cells provides an important understanding of how neurogenesis is maintained in the adult brain.

Materials and Methods

Animals. Mice were housed and treated according to the guidelines from the University of California, San Francisco Laboratory Animal Care and Use Committee. Three hundred seventy-six 2-month-old male C57/BL6 (Charles River) mice were used for all of the controls of the DA and the study of C and A cells. For B1 cell analysis, we used 109 hGFAP::GFP mice (FVB/N-TgGFAPGFP14Mes/J; Jackson Labs). (For a complete list of mouse strains and primers used for genotyping, see Table S1.) This many animals were required because from each animal only two whole-mount preparations can be obtained.

Whole-Mount Preparation. Mice were deeply anesthetized with 13 mg/kg BW tribromoethanol (Avertin) and perfused transcardially with 0.9% NaCl. Brains were removed, and the lateral and medial ventricular walls were immediately dissected out in warm Leibovitz's L15 medium as published previously (3, 17, 70). In all of the experiments described here, whole mounts were fixed in 4% paraformaldehyde and 0.1% Triton for 6 h and then kept in PBS-sodium azide at 4 °C until immunohistochemical processing.

Whole mounts were incubated for 48 h at 4 °C with primary antibodies, followed by 48 h at 4 °C with the appropriate secondary antibodies (Table S2). For mounting, whole mounts were then further dissected and embedded with Aqua Poly/Mount mounting medium (Polysciences).

Cell Quantifications. Images of defined V-SVZ subregions (Fig. S1*A*) were acquired with a Leica SP5 confocal microscope (Leica). Both hemispheres of five animals for each time point were analyzed. Four nonoverlapping high-power fields (386 × 386 μm^2) of the lateral wall of the V-SVZ corresponding to the anterior dorsal (AD), anterior ventral (AV), posterior dorsal (PD), posterior ventral (PV), and one AV field in the medial wall (MV) were analyzed for each hemisphere (Fig. S1*A*).

Double- and triple-labeled cells were counted tridimensionally using the Imaris software (Imaris; Bitplane). All values are expressed as number of cells per square millimeter or as ratios. Data were analyzed by Student's *t* test, with a value of $P \leq 0.05$ considered statistically significant.

Thymidine Analogs. CldU (Sigma) and EdU (Invitrogen) were dissolved at 10 mg/mL in sterile PBS and administered by an i.p. injection. Because their molecular weight is similar (CldU, 262.65 g/mol; EdU, 252.22 g/mol), we used the same dose of 50 mg/kg for both analogs.

For CldU labeling, samples were pretreated with formamide SSC (20), denatured with 0.5 M hydrochloric acid for 30 min at 37 °C, washed with boric buffer for 10 min, and processed for rat anti-BrdU antibody staining (Table S1). EdU was detected using a commercial kit (Invitrogen) at the end of the immunohistochemical reactions.

In vivo controls. Mice received subsequently one injection of CldU and one of EdU 2 h later or vice versa and were killed after 30 min. Alternatively, mice received either one injection of CldU or EdU, or both (50 mg/kg), 30 min before fixation. Whole mounts were prepared and stained as explained above. The average number of cells per square millimeter labeled by EdU was compared with the counts for CldU labeling. Both analogs had the same efficiency with little or no cross-reaction between them.

Moreover, to ensure that the labeling with CldU did not impair the ability of cells to incorporate EdU 2 h later, we counted the number of EdU-labeled cells 30 min after the injection in mice that received only EdU to mice previously treated with CldU.

Evaluation of the toxicity of thymidine analogs. Primary cultures were prepared from the V-SVZ from mice that received EdU in vivo 1 h before the dissection and analyzed for EdU-labeling 2 and 24 h later but not from CldU-treated mice. Plates were fixed 2 and 24 h later and stained for either CldU or EdU. In addition, C57/BL6 mice received either one injection of CldU or EdU (50 mg/kg) and were killed at different time points. Whole mounts were processed as described above. The number of labeled cells was counted along with the number of labeled Ascl1$^+$ cells (Fig. S1 *B–I*).

Cell Cycle Determination. All of the cell cycle analysis experiments started at 0900 hours.

CL method. Two-month-old mice (C57/BL6; hGFAP::GFP) received 1–16 repeated injections of EdU (50 mg/kg, one every 2 h). Two hours is shorter than the S phase for V-SVZ cells (*Results*), assuring that all V-SVZ cells dividing during the experiment would be labeled by EdU (16). Mice were killed 30 min after the last injection, and the lateral and medial wall of the lateral ventricle were dissected. Whole mounts were stained for either GFP or Ascl1 and EdU (as described above).

For each time point, five mice (10 hemispheres) were analyzed. EdU$^+$, GFP$^+$ (or Ascl1$^+$), and double-labeled cells within five subregions of the V-SVZ (Fig. S1*A*) were acquired in z stacks with the confocal microscope and quantified using Imaris software.

The labeled fraction of a population (number of hGFAP::GFP$^+$EdU$^+$ or Ascl1$^+$EdU$^+$ cells divided by the total number of hGFAP::GFP$^+$ or Ascl1$^+$ cells, respectively) was counted, and the labeling indexes (16) were determined and averaged for each survival time. CL data can be described by two regression lines: line a, least-squares fit lines through the data points prior the plateau of LI; line b, the plateau y = GF (Figs. 2 *A–E* and 3 *A–D*). The intersect of the first regression line with the y axis is defined as the initial labeling index (LI_0) and corresponds to (GF × T_S)/T_C (16, 34). The time (x axis) at which the plateau is reached (when the two regression lines intersect) equals $T_C - T_S$.

By resolving the two equations a) and b) we calculated T_C and T_S.

DA method. Two-month-old mice were injected intraperitoneally with 50 mg/kg of CldU. Two hours (hGFAP::GFP $n = 5$) or 3 h (C57/BL6 $n = 10$) later, we injected EdU at the same dose, killed the mice 30 min later, and prepared whole mounts. Whole mounts were immunostained for cell type-specific markers (GFP, Ascl1, or DCX), and CldU and EdU were detected as described above. In each population (B1, C, A cells), the ratio between the cells labeled only by CldU (or by EdU) to the total population (GFP^+ or $Ascl1^+$ or DCX) was determined (Figs. 2 *F–H*, 3 *E* and *F*, and 4 *A* and *B*). Cells that had exited the S phase between the two injections were labeled only by the first analog, whereas the total number of cells in the S phase were labeled by the second analog. The ratio of these two values is equal to the ratio of the interval between the two injections over the length of the S phase (for each cell type: $CldU^+EdU^-/EdU^+ = 3\ h/T_S$). From this equation we estimated T_S.

PLM method. Mice received a single injection of 50mg/kg CldU, and whole mounts were prepared after different time points [hGFAP::GFP mice were killed at 30 min and 2, 4, 6, and 8 h; C57/BL6 mice were killed at 30 min and 2, 4, 6, 8, 10, 12, 14, 16, 18, 20, 22, 24, 26, 28, 30, 36, 42, 48, 54, 60, 66, 72 h after CldU injection; (Figs. 3 *G–K* and 4 *C–E* and Fig. S1*W*)]. For each population (B1, C, A cells) the number of mitotic ($pHH3^+$) cells and mitotic $CldU^+$ cells were measured for each time point. Nuclei with a homogeneous staining for pHH3 were counted as labeled mitosis (Fig. 3*H*). Nuclei with few bright discrete dots of nuclear pHH3 labeling were not counted as these correspond to cells that are still in the G_2 phase (71).

For each cell type, we calculated the ratio of $CldU^+$-labeled mitoses to the total number of mitoses (e.g., $Ascl1^+CldU^+pHH3^+/Ascl1^+pHH3^+$) for each time point. The values of this time course were plotted and described by regression lines.

By calculating the least square fit for the ascending, plateau, and descending lines, we can calculate (33): T_{G2} (line a; $y = 0$), $T_{G2} + T_M$ (line a for $y = 1$), $T_{G2} + T_M + T_S$ (line b; $y = 0$), T_C [difference from the middle of the line c ($y = 0.36$) and the middle of the line a ($y = 0.50$); Fig. 3 *G–I*].

Estimations of the Number of C Cell Divisions. Two-month-old mice (C57/BL6; $n = 69$) received one initial injection of CldU (50mg/kg), followed at different intervals by one EdU injection (50 mg/kg). Mice were killed 30 min after the EdU injection ($n = 3$ for each time point). Whole mounts were stained for Ascl1, CldU, and EdU.

Cells that were only labeled by CldU (EdU^-) correspond to cells that underwent S phase at $t = 0$, progressed through the cell cycle, and were in a different cell cycle phase at the time of EdU injection (see above). By analyzing the ratio of $Ascl1^+CldU^+EdU^-/Ascl1^+EdU^+$ cells at different time points, we estimated the number of times a cohort of cells reenters the S phase (i.e., incorporated EdU). At short intervals between the two analog administrations, most of the $Ascl1^+CldU^+$ cells are also labeled by EdU. The number of $Ascl1^+CldU^+EdU^-$ cells increased as the cohort of $CldU^+$ cells exited S phase and decreased again at longer time points as these cells reentered S phase. Every time the cohort of cells underwent a S phase, the ratio $Ascl1^+CldU^+EdU^-/Ascl1^+EdU^+$ reached a minimum. From the number of troughs, we estimated the number of cell divisions of the C cell population, and from the intervals between them, we estimated T_C.

ACKNOWLEDGMENTS. We thank L. Fuentealba, D. Hansen, Y.-G. Han, R. Ihrie, T. Nguyen, C. Harwell, F. Luzzati, A. Buffo, and C. Rolando for discussions. We also thank two anonymous reviewers who made insightful suggestions to improve a previous version of this paper. This work was supported by National Institutes of Health Grant NS-28478, the John G. Bowes Research Fund, the European Community's Seventh Framework Programme (FP7/2007-2013) under Grant Agreement 220005, and Regione Piemonte "Ricerca Sanitaria Finalizzata 2008." A.A.-B. is the Heather and Melanie Muss Endowed Chair of Neurological Surgery at the University of California, San Francisco. G.P. is supported by the European Community's Seventh Framework Programme (FP7/2007-2013) under Grant Agreement 220005. K.O. is supported by the German Research Foundation (Deutsche Forschungsgemeinschaft).

1. Doetsch F, Caillé I, Lim DA, García-Verdugo JM, Alvarez-Buylla A (1999) Subventricular zone astrocytes are neural stem cells in the adult mammalian brain. *Cell* 97(6): 703–716.
2. Lim DA, et al. (2000) Noggin antagonizes BMP signaling to create a niche for adult neurogenesis. *Neuron* 28(3):713–726.
3. Mirzadeh Z, Merkle FT, Soriano-Navarro M, Garcia-Verdugo JM, Alvarez-Buylla A (2008) Neural stem cells confer unique pinwheel architecture to the ventricular surface in neurogenic regions of the adult brain. *Cell Stem Cell* 3(3):265–278.
4. Fuentealba LC, Obernier K, Alvarez-Buylla A (2012) Adult neural stem cells bridge their niche. *Cell Stem Cell* 10(6):698–708.
5. Luskin MB, Zigova T, Soteres BJ, Stewart RR (1997) Neuronal progenitor cells derived from the anterior subventricular zone of the neonatal rat forebrain continue to proliferate in vitro and express a neuronal phenotype. *Mol Cell Neurosci* 8(5):351–366.
6. Lois C, García-Verdugo JM, Alvarez-Buylla A (1996) Chain migration of neuronal precursors. *Science* 271(5251):978–981.
7. Menezes JR, Smith CM, Nelson KC, Luskin MB (1995) The division of neuronal progenitor cells during migration in the neonatal mammalian forebrain. *Mol Cell Neurosci* 6(6):496–508.
8. Petreanu L, Alvarez-Buylla A (2002) Maturation and death of adult-born olfactory bulb granule neurons: Role of olfaction. *J Neurosci* 22(14):6106–6113.
9. Imayoshi I, et al. (2008) Roles of continuous neurogenesis in the structural and functional integrity of the adult forebrain. *Nat Neurosci* 11(10):1153–1161.
10. Lazarini F, Lledo PM (2011) Is adult neurogenesis essential for olfaction? *Trends Neurosci* 34(1):20–30.
11. Morshead CM, van der Kooy D (1992) Postmitotic death is the fate of constitutively proliferating cells in the subependymal layer of the adult mouse brain. *J Neurosci* 12(1):249–256.
12. Lewis PD (1968) A quantitative study of cell proliferation in the subependymal layer of the adult rat brain. *Exp Neurol* 20(2):203–207.
13. Sajad M, et al. (2011) Cytokinetics of adult rat SVZ after EAE. *Brain Res* 1371:140–149.
14. Schultze B, Korr H (1981) Cell kinetic studies of different cell types in the developing and adult brain of the rat and the mouse: A review. *Cell Tissue Kinet* 14(3):309–325.
15. Lois C, Alvarez-Buylla A (1994) Long-distance neuronal migration in the adult mammalian brain. *Science* 264(5162):1145–1148.
16. Nowakowski RS, Lewin SB, Miller MW (1989) Bromodeoxyuridine immunohistochemical determination of the lengths of the cell cycle and the DNA-synthetic phase for an anatomically defined population. *J Neurocytol* 18(3):311–318.
17. Mirzadeh Z, Doetsch F, Sawamoto K, Wichterle H, Alvarez-Buylla A (2010) The subventricular zone en-face: Wholemount staining and ependymal flow. *J Vis Exp* (39):e1938.
18. Merkle FT, Mirzadeh Z, Alvarez-Buylla A (2007) Mosaic organization of neural stem cells in the adult brain. *Science* 317(5836):381–384.
19. De Marchis S, et al. (2007) Generation of distinct types of periglomerular olfactory bulb interneurons during development and in adult mice: Implication for intrinsic properties of the subventricular zone progenitor population. *J Neurosci* 27(3): 657–664.
20. Leuner B, Glasper ER, Gould E (2009) Thymidine analog methods for studies of adult neurogenesis are not equally sensitive. *J Comp Neurol* 517(2):123–133.
21. Taupin P (2007) BrdU immunohistochemistry for studying adult neurogenesis: Paradigms, pitfalls, limitations, and validation. *Brain Res Brain Res Rev* 53(1):198–214.
22. Belluzzi O, Benedusi M, Ackman J, LoTurco JJ (2003) Electrophysiological differentiation of new neurons in the olfactory bulb. *J Neurosci* 23(32):10411–10418.
23. Parras CM, et al. (2004) Mash1 specifies neurons and oligodendrocytes in the postnatal brain. *EMBO J* 23(22):4495–4505.
24. Nacher J, Crespo C, McEwen BS (2001) Doublecortin expression in the adult rat telencephalon. *Eur J Neurosci* 14(4):629–644.
25. Zhuo L, et al. (1997) Live astrocytes visualized by green fluorescent protein in transgenic mice. *Dev Biol* 187(1):36–42.
26. Platel JC, Gordon V, Heintz T, Bordey A (2009) GFAP-GFP neural progenitors are antigenically homogeneous and anchored in their enclosed mosaic niche. *Glia* 57(1): 66–78.
27. Doetsch F, García-Verdugo JM, Alvarez-Buylla A (1997) Cellular composition and three-dimensional organization of the subventricular germinal zone in the adult mammalian brain. *J Neurosci* 17(13):5046–5061.
28. Pastrana E, Cheng LC, Doetsch F (2009) Simultaneous prospective purification of adult subventricular zone neural stem cells and their progeny. *Proc Natl Acad Sci USA* 106(15):6387–6392.
29. Kim Y, et al. (2010) Dopamine stimulation of postnatal murine subventricular zone neurogenesis via the D3 receptor. *J Neurochem* 114(3):750–760.
30. Sarli G, Benazzi C, Preziosi R, Marcato PS (1994) Proliferative activity assessed by anti-PCNA and Ki67 monoclonal antibodies in canine testicular tumours. *J Comp Pathol* 110(4):357–368.
31. Hayes NL, Nowakowski RS (2000) Exploiting the dynamics of S-phase tracers in developing brain: Interkinetic nuclear migration for cells entering versus leaving the S-phase. *Dev Neurosci* 22(1-2):44–55.
32. Nowakowski RS, Caviness VS, Jr., Takahashi T, Hayes NL (2002) Population dynamics during cell proliferation and neuronogenesis in the developing murine neocortex. *Results Probl Cell Differ* 39:1–25.
33. Cai L, Hayes NL, Nowakowski RS (1997) Local homogeneity of cell cycle length in developing mouse cortex. *J Neurosci* 17(6):2079–2087.
34. Takahashi T, Nowakowski RS, Caviness VS, Jr. (1993) Cell cycle parameters and patterns of nuclear movement in the neocortical proliferative zone of the fetal mouse. *J Neurosci* 13(2):820–833.
35. Young KM, Fogarty M, Kessaris N, Richardson WD (2007) Subventricular zone stem cells are heterogeneous with respect to their embryonic origins and neurogenic fates in the adult olfactory bulb. *J Neurosci* 27(31):8286–8296.
36. Menezes JR, Luskin MB (1994) Expression of neuron-specific tubulin defines a novel population in the proliferative layers of the developing telencephalon. *J Neurosci* 14(9):5399–5416.
37. Chiasson BJ, Tropepe V, Morshead CM, van der Kooy D (1999) Adult mammalian forebrain ependymal and subependymal cells demonstrate proliferative potential, but only subependymal cells have neural stem cell characteristics. *J Neurosci* 19(11): 4462–4471.
38. Takahashi T, Nowakowski RS, Caviness VS, Jr. (1995) The cell cycle of the pseudostratified ventricular epithelium of the embryonic murine cerebral wall. *J Neurosci* 15(9):6046–6057.

39. Kriegstein A, Alvarez-Buylla A (2009) The glial nature of embryonic and adult neural stem cells. *Annu Rev Neurosci* 32:149–184.
40. Cooper-Kuhn CM, Kuhn HG (2002) Is it all DNA repair? Methodological considerations for detecting neurogenesis in the adult brain. *Brain Res Dev Brain Res* 134(1-2):13–21.
41. Breunig JJ, Arellano JI, Macklis JD, Rakic P (2007) Everything that glitters isn't gold: A critical review of postnatal neural precursor analyses. *Cell Stem Cell* 1(6):612–627.
42. Zeng C, et al. (2010) Evaluation of 5-ethynyl-2′-deoxyuridine staining as a sensitive and reliable method for studying cell proliferation in the adult nervous system. *Brain Res* 1319:21–32.
43. Smith CM, Luskin MB (1998) Cell cycle length of olfactory bulb neuronal progenitors in the rostral migratory stream. *Dev Dyn* 213(2):220–227.
44. Thomaidou D, Mione MC, Cavanagh JF, Parnavelas JG (1997) Apoptosis and its relation to the cell cycle in the developing cerebral cortex. *J Neurosci* 17(3): 1075–1085.
45. Yang HK, et al. (2004) Distribution of doublecortin expressing cells near the lateral ventricles in the adult mouse brain. *J Neurosci Res* 76(3):282–295.
46. Ishii Y, et al. (2008) Characterization of neuroprogenitor cells expressing the PDGF beta-receptor within the subventricular zone of postnatal mice. *Mol Cell Neurosci* 37(3):507–518.
47. Anthony TE, Heintz N (2008) Genetic lineage tracing defines distinct neurogenic and gliogenic stages of ventral telencephalic radial glial development. *Neural Dev* 3:30.
48. Cahoy JD, et al. (2008) A transcriptome database for astrocytes, neurons, and oligodendrocytes: A new resource for understanding brain development and function. *J Neurosci* 28(1):264–278.
49. Regan MR, et al. (2007) Variations in promoter activity reveal a differential expression and physiology of glutamate transporters by glia in the developing and mature CNS. *J Neurosci* 27(25):6607–6619.
50. Yang Y, et al. (2011) Molecular comparison of GLT1+ and ALDH1L1+ astrocytes in vivo in astroglial reporter mice. *Glia* 59(2):200–207.
51. Castro DS, et al. (2011) A novel function of the proneural factor Ascl1 in progenitor proliferation identified by genome-wide characterization of its targets. *Genes Dev* 25(9):930–945.
52. Baek JH, Hatakeyama J, Sakamoto S, Ohtsuka T, Kageyama R (2006) Persistent and high levels of Hes1 expression regulate boundary formation in the developing central nervous system. *Development* 133(13):2467–2476.
53. Costa MR, et al. (2011) Continuous live imaging of adult neural stem cell division and lineage progression in vitro. *Development* 138(6):1057–1068.
54. Doetsch F, García-Verdugo JM, Alvarez-Buylla A (1999) Regeneration of a germinal layer in the adult mammalian brain. *Proc Natl Acad Sci USA* 96(20):11619–11624.
55. Richardson SJ, Lemkine GF, Alfama G, Hassani Z, Demeneix BA (2007) Cell division and apoptosis in the adult neural stem cell niche are differentially affected in transthyretin null mice. *Neurosci Lett* 421(3):234–238.
56. Menn B, et al. (2006) Origin of oligodendrocytes in the subventricular zone of the adult brain. *J Neurosci* 26(30):7907–7918.
57. Gonzalez-Perez O, Romero-Rodriguez R, Soriano-Navarro M, Garcia-Verdugo JM, Alvarez-Buylla A (2009) Epidermal growth factor induces the progeny of subventricular zone type B cells to migrate and differentiate into oligodendrocytes. *Stem Cells* 27(8):2032–2043.
58. Singh SK, et al. (2004) Identification of human brain tumour initiating cells. *Nature* 432(7015):396–401.
59. Woo RA, Poon RY (2003) Cyclin-dependent kinases and S phase control in mammalian cells. *Cell Cycle* 2(4):316–324.
60. Kastan MB, Lim DS (2000) The many substrates and functions of ATM. *Nat Rev Mol Cell Biol* 1(3):179–186.
61. Alexiades MR, Cepko C (1996) Quantitative analysis of proliferation and cell cycle length during development of the rat retina. *Dev Dyn* 205(3):293–307.
62. Lakhotia SC, Sinha P (1983) Replication in Drosophila chromosomes. X. Two kinds of active replicons in salivary gland polytene nuclei and their relation to chromosomal replication patterns. *Chromosoma* 88(4):265–276.
63. Shaw A, Olivares-Chauvet P, Maya-Mendoza A, Jackson DA (2010) S-phase progression in mammalian cells: Modelling the influence of nuclear organization. *Chromosome Res* 18(1):163–178.
64. Herrick J (2011) Genetic variation and DNA replication timing, or why is there late replicating DNA? *Evolution* 65(11):3031–3047.
65. Calegari F, Huttner WB (2003) An inhibition of cyclin-dependent kinases that lengthens, but does not arrest, neuroepithelial cell cycle induces premature neurogenesis. *J Cell Sci* 116(Pt 24):4947–4955.
66. Lange C, Huttner WB, Calegari F (2009) Cdk4/cyclinD1 overexpression in neural stem cells shortens G1, delays neurogenesis, and promotes the generation and expansion of basal progenitors. *Cell Stem Cell* 5(3):320–331.
67. Calegari F, Haubensak W, Haffner C, Huttner WB (2005) Selective lengthening of the cell cycle in the neurogenic subpopulation of neural progenitor cells during mouse brain development. *J Neurosci* 25(28):6533–6538.
68. Hodge RD, D'Ercole AJ, O'Kusky JR (2004) Insulin-like growth factor-I accelerates the cell cycle by decreasing G1 phase length and increases cell cycle reentry in the embryonic cerebral cortex. *J Neurosci* 24(45):10201–10210.
69. Salomoni P, Calegari F (2010) Cell cycle control of mammalian neural stem cells: Putting a speed limit on G1. *Trends Cell Biol* 20(5):233–243.
70. Doetsch F, Alvarez-Buylla A (1996) Network of tangential pathways for neuronal migration in adult mammalian brain. *Proc Natl Acad Sci USA* 93(25):14895–14900.
71. Hendzel MJ, et al. (1997) Mitosis-specific phosphorylation of histone H3 initiates primarily within pericentromeric heterochromatin during G2 and spreads in an ordered fashion coincident with mitotic chromosome condensation. *Chromosoma* 106(6):348–360.